

## REDSHIFTS IN THE SOUTHERN ABELL REDSHIFT SURVEY CLUSTERS. I. THE DATA

M. J. WAY,<sup>1,2</sup> H. QUINTANA,<sup>2</sup> L. INFANTE,<sup>2</sup> D. G. LAMBAS,<sup>3,4</sup> AND H. MURIEL<sup>3,4</sup>

Received 2005 January 3; accepted 2005 June 24

### ABSTRACT

The Southern Abell Redshift Survey (SARS) contains 39 clusters of galaxies with redshifts in the range  $0.0 < z < 0.31$  and a median redshift depth of  $\bar{z} = 0.0845$ . SARS covers the region  $0^\circ < \delta < -65^\circ$ ,  $\alpha < 5^{\text{h}}$ ,  $\alpha > 21^{\text{h}}$  (while avoiding the LMC and SMC), with  $|b| > 40^\circ$ . Cluster locations were chosen from the Abell and Abell-Corwin-Olowin catalogs, while galaxy positions were selected from the Automatic Plate Measuring Facility galaxy catalog with extinction-corrected magnitudes in the range  $15 \leq b_J < 19$ . SARS used the Las Campanas 2.5 m du Pont telescope, observing either 65 or 128 objects concurrently over a  $1.5 \text{ deg}^2$  field. New redshifts for 3440 galaxies are reported in the fields of these 39 clusters of galaxies.

*Key words:* galaxies: clusters: general — galaxies: distances and redshifts

*Online material:* machine-readable table

### 1. INTRODUCTION

Clusters of galaxies appear as nodes in a gravitationally unfolding web of dark matter, dark energy, and baryons that represents the large-scale structure of our universe. These nodes are, in fact, still forming in the present epoch. Therefore, local observations of clusters of galaxies in comparison with those at higher redshift (e.g., Castillo-Morales & Schindler 2003) in the context of large cosmological simulations (e.g., Kochanek et al. 2003) may in principle lead to a better understanding of the physical conditions in the early universe.

In order to characterize the clustering of galaxies on multiple scales, many statistical techniques have been used over the years. For example, using strictly position and velocity information as contained in the Southern Abell Redshift Survey (SARS), some in wide use are the cross-correlation function  $\xi(r)$  (Peebles 1980), the Lee statistic (Fitchett 1988), the  $\Delta$ -test (Dressler & Schectman 1988), the  $\alpha$ -test (West & Bothun 1990), the  $\epsilon$ -test (Bird 1994), minimal spanning trees (Doroshkevich et al. 2004), extended friends-of-friends algorithms (Botzler et al. 2004), percolation algorithms (Adami & Mazure 2002), and even Minkowski functionals (Schmalzing et al. 1999) to name but a few. However, galaxy velocities in clusters have been traditionally hard to obtain when one wants to reach volumes and numbers large enough to study a statistically representative sample of the universe. To contribute toward this need, redshift data in the fields of 39 clusters of galaxies have been collected during several observing sessions over 3 years to carry out dynamical and morphological analyses.

The SARS cluster positions were selected from the Abell (Abell 1958) and Abell-Corwin-Olowin (ACO; Abell et al. 1989) catalogs. Galaxy positions were taken from the Automatic Plate Measuring (APM)  $b_J$  catalog (Maddox et al. 1990a, 1990b, 1996).

For a discussion of the velocity dispersions and cluster dynamics in these clusters, see Muriel et al. (2002, hereafter Paper II). For information related to the individual galaxy luminosity profiles in SARS, see Coenda et al. (2005a, 2005b).

Cluster selection is discussed in § 2, galaxy selection from the APM in § 3, spectral data observations in § 4, spectral reductions and velocity data results in § 5, survey completeness in § 6, and cluster identification in § 7, and we summarize in § 8.

### 2. THE CLUSTER SAMPLE

Clusters of richness  $R \geq 0$  were selected<sup>5</sup> from the Abell and ACO catalogs in the region  $0^\circ < \delta < -65^\circ$ ,  $\alpha < 5^{\text{h}}$ ,  $\alpha > 21^{\text{h}}$  (avoiding the LMC and SMC), with  $|b| > 40^\circ$ , in the distance range represented by Abell distance classes 4 and 5, so that most of the clusters were covered by the du Pont Telescope fiber spectrograph  $1.5 \text{ deg}^2$  field. Our program was designed to observe a complete sample in a defined volume near the south Galactic pole while observing clusters within a reasonable spread of right ascension and declination for observing accessibility from telescopes in Chile. Our original observing goals were not met for two reasons: (1) our program was not granted sufficient time at the Las Campanas Observatory (LCO) 2.5 m telescope; and (2) our original program was meant to include the use of the 4 m telescope at Cerro Tololo Inter-American Observatory (CTIO), and we were unsuccessful in obtaining those observations. Therefore, SARS is not a complete sample of the clusters of galaxies in the sample volume.

One of the original goals of the project was to measure the two-point correlation function  $\xi(r)$  of clusters of galaxies. The estimate of  $\xi(r)$  depends strongly on edge corrections. If one selects the objects just by the Abell distance class, the distant (higher redshift) edge of the cone will have an irregular shape and be ill defined because the spread of the distance distributions for  $D = 5$  and 6 are wide and mixed (Quintana & White 1990). To avoid this problem, the distance was estimated by using a combination of magnitudes and distance classes to a depth of  $z \approx 0.17$ . The final determination of the near and far distance limit was to be precisely defined after the galaxy redshifts were acquired.

<sup>1</sup> Space Sciences Division, NASA Ames Research Center, MS 245-6, Moffett Field, CA 94035.

<sup>2</sup> Department of Astronomy and Astrophysics, Pontificia Universidad Católica de Chile, Casilla 306, Santiago 22, Chile.

<sup>3</sup> Grupo de Investigaciones en Astronomía Teórica y Experimental, Observatorio Astronómico, Laprida 854, 5000 Córdoba, Argentina.

<sup>4</sup> CONICET, Avenida Rivadavia 1917, CP C1033AAJ Buenos Aires, Argentina.

<sup>5</sup> The statement by Muriel et al. (2002) that only Abell clusters of  $R > 0$  are included in the sample is incorrect.

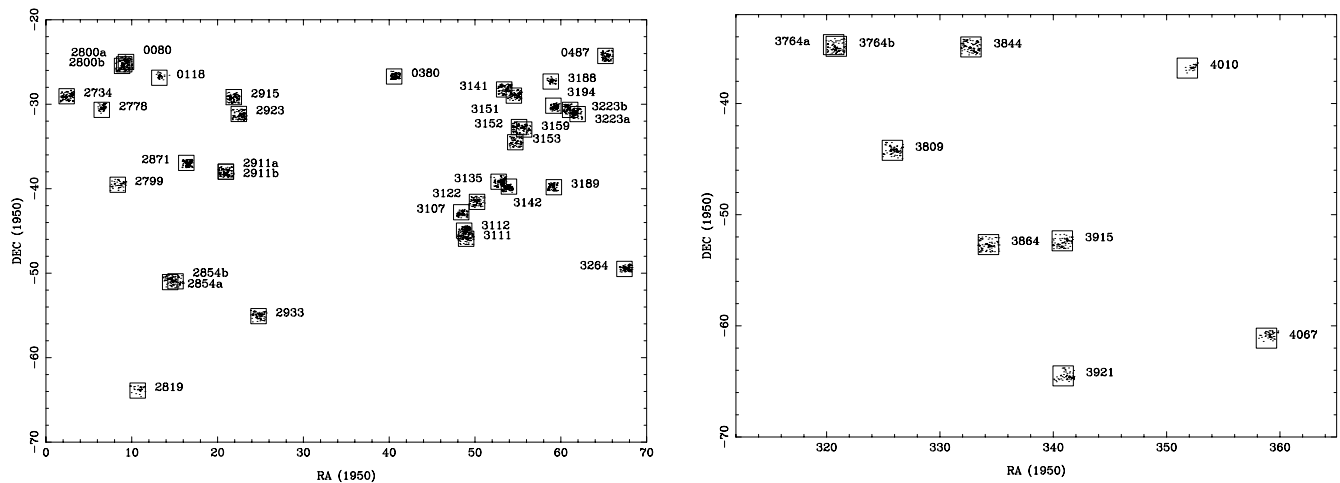


FIG. 1.—Measured galaxy velocities with plate centers and  $1.5 \text{ deg}^2$  squares overlaid for all clusters. *Left*: R.A. =  $0^{\text{h}}$  to  $4^{\text{h}}40^{\text{m}}$ , decl. =  $-20^{\circ}$  to  $-70^{\circ}$  (B1950.0). *Right*: R.A. =  $21^{\text{h}}20^{\text{m}}$  to  $24^{\text{h}}$ , decl. =  $-32^{\circ}$  to  $-70^{\circ}$  (B1950.0).

To have the full Abell diameter area within the field of view of the two telescopes originally proposed for use in this project (the CTIO 4 m and the LCO 2.5 m), we set the low-redshift side of the volume to be  $15,000 \text{ km s}^{-1}$ . This choice also avoids the small number statistics in cluster density on the low-redshift side of the survey volume cone.

The selected volume of the universe was also chosen to avoid problems with Milky Way obscuration and differences between north and south. The observed sample represents a nearly random selection of clusters in the defined area with a rather even distribution in right ascension, as needed for telescope observing accessibility (see Fig. 1).

The catalog can be shown to be broadly representative of the Abell and ACO catalogs in a number of ways. The catalog contains a broad range of Bautz-Morgan types (Table 1, col. [5]), although it is slightly biased toward high classes. Also, the regular/irregular types (Table 1, col. [4]) as defined by Abell are represented. The catalog also attempts to provide redshifts for galaxies in moderately rich clusters (Table 1, col. [7]), not only in the very richest systems. This makes SARS useful for studying the properties of clusters corresponding to a wide range of masses in a nearby sample.

Table 1 lists the information for each observation with the fiber spectrograph. Column (1) gives the Abell number, columns (2) and (3) the right ascension in hours and declination in degrees, column (4) the Abell classification, column (5) the Bautz-Morgan type, column (6) the Abell number counts, column (7) the Abell richness class, column (8) the Abell distance class, column (9) the magnitude of the tenth-brightest red cluster galaxy (from the Abell and ACO catalogs), column (10) the date of the observations, and column (11) the final number of galaxies per cluster field (stars and duplicate measurements are removed).

### 3. THE APM GALAXY SAMPLE

The galaxies were selected from the APM  $b_J$  catalog (Maddox et al. 1990a, 1990b, 1996). The extended version of the APM galaxy catalog contains over 5 million galaxies brighter than  $b_J = 20.5$  over the north and south Galactic poles, covering nearly  $10^4 \text{ deg}^2$ . It was based on 390 contiguous UK Schmidt Telescope J survey plates. The image surface brightness profiles were used to distinguish galaxies from stars and merged images. Extensive visual checks were performed to quantify the completeness of the galaxy sample and contamination from stellar images. Galaxies

in the SARS sample were selected in the range  $15 \leq b_J < 19$  and were within  $1.5 \text{ deg}^2$  of the cluster center.<sup>6</sup> This is the field of view of the LCO 2.5 m fiber spectrograph. Galaxies were also always chosen within 1 Abell radius of the center. For the first observing session, galaxies were chosen in order of decreasing APM magnitude such that a significant number over the number of available fibers was available for selection. This was needed, since the software that allocates fibers to galaxies discards targets that are within  $\sim 30''$  of another target or are too close to the center of the plate (where there is a centering hole). This strategy obviously produced too many galaxy targets belonging to groups in the foreground of the cluster. In trying to optimize the use of the fibers in subsequent telescope sessions, we decided to identify the brightest cluster member and chose galaxies fainter than that. However, to check on the procedure we choose a few brighter galaxies that should have been foreground galaxies. A secondary criteria for target selection was to avoid objects whose images seemed to be of very low surface brightness, since the resulting spectrum would have insufficient signal-to-noise ratio (S/N) to be useful. All these procedures allowed optimal use of the 65 (and later 128) fibers used to collect the spectra. The APM positions are listed in Table 2 and are internally accurate to within  $0''.5$ .

### 4. SPECTRAL OBSERVATIONS

Spectroscopic observations were carried out with the 2.5 m du Pont Telescope of LCO, Chile. The original multifiber spectrograph (Shectman 1989, 1993) consisted of a plug plate at the focal plane to which 65 fibers were attached and run to a Boller & Chivens spectrograph coupled to a 2D-Fruitti instrument. The 2D-Fruitti instrument has a blue-sensitive Carnegie image tube as the first stage followed by a middle stage consisting of a series of microchannel plates ending with a continuously read rocking CCD. A  $600 \text{ line mm}^{-1}$  grating blazed at  $5000 \text{ \AA}$  was set at an angle of  $9^{\circ} 40'$ , giving wavelength coverage from  $\sim 3800$  to  $6800 \text{ \AA}$ . Normally, 50–55 fibers were used for objects. Ten sky fibers were set aside, spaced at intervals of one every six fibers along the spectrograph entrance and positioned in a random pattern in the plug plate. The resulting 2D-Fruitti image had a  $1520 \times 1024$  pixel area, with a dispersion

<sup>6</sup> Muriel et al. (2002) state that the SARS sample only included galaxies brighter than  $m_R = 19$ . This is mistaken, as the original APM survey is in  $b_J$  and galaxies were selected in the range of  $15 \leq b_J < 19$ .

TABLE 1  
CLUSTER OBSERVATIONS: SPECTROSCOPY

Abell (1)	R.A. (B1950.0) (2)	Decl. (B1950.0) (3)	Type <sup>a</sup> (4)	Bautz-Morgan (5)	Counts <sup>b</sup> (6)	Richness Class (7)	Distance Class (8)	$m_{10}$ <sup>c</sup> (9)	Date Observed (10)	Number <sup>d</sup> (11)
0080.....	0.63167	-24.95000	I	III	64	0	4	15.8	1993 Oct	107
0118.....	0.88833	-26.68333	I	II-III	77	1	5	17.2	1991 Sep	36
0380.....	2.70333	-26.46667	RI	II	64	2	5	17.2	1991 Nov	99
0487.....	4.34603	-24.28309	I	II-III	104	2	5	17.2	1992 Jan	85
2734.....	0.14667	-29.15000	R	III	58	1	4	16.3	1993 Oct	104
2778.....	0.43500	-30.51667	I	III	51	1	5	17.0	1991 Sep	48
2799.....	0.58500	-39.40000	RI	I-II	63	1	4	16.2	1991 Sep	48
2800.....	0.59167	-25.36667	I	III	59	1	4	15.8	1991 Sep, 1993 Sep	119
2819.....	0.72833	-63.86667	R	I-II	90	2	4	16.0	1991 Sep	47
2854.....	0.97667	-50.80000	RI	I-II	64	1	4	15.8	1991 Sep, 1993 Sep	105
2871.....	1.09333	-37.00000	R	I	92	2	5	16.7	1991 Nov	104
2911.....	1.39667	-38.23333	R	I-II	72	1	4	16.3	1991 Sep, 1993 Sep	123
2915.....	1.44167	-29.26667	I	II	55	1	5	16.9	1991 Nov	104
2923.....	1.50000	-31.35000	RI	I-II	50	1	5	17.0	1991 Nov	110
2933.....	1.64667	-54.81667	RI	III	77	1	5	16.9	1993 Oct	95
3107.....	3.22667	-42.95000	IR	II	61	1	5	17.0	1992 Dec	77
3111.....	3.26833	-45.91667	R	I-II	54	1	4	16.3	1991 Nov	110
3112.....	3.27000	-44.41667	R	I	116	2	4	16.1	1992 Jan	106
3122.....	3.34167	-41.51667	R	I-II	100	2	4	15.8	1992 Jan	87
3135.....	3.53667	-39.16667	R	II	111	2	3	15.5	1991 Nov	109
3141.....	3.58167	-28.21667	RI	II-III	55	1	5	16.8	1992 Jan	96
3142.....	3.58167	-39.96667	RI	I-II	78	1	5	16.9	1991 Nov	110
3151.....	3.64000	-28.86667	R	I-II	52	1	4	16.0	1991 Nov	101
3152.....	3.64000	-32.73333	RI	I-II	51	1	5	17.0	1992 Jan	53
3153.....	3.65167	-34.41667	I	I-II	64	1	5	17.0	1992 Dec	73
3159.....	3.70167	-32.85000	RI	I-II	98	2	5	17.1	1992 Dec	68
3188.....	3.92833	-27.18333	I	III	67	1	5	17.1	1992 Dec	46
3189.....	3.93333	-39.75000	RI	II	65	1	6	17.4	1992 Dec	85
3194.....	3.95333	-30.31667	I	III	83	2	5	16.7	1992 Jan	94
3223.....	4.11000	-30.95000	RI	I	100	2	3	15.6	1991 Nov, 1992 Dec	196
3264.....	4.50167	-49.41667	I	II	53	1	5	16.7	1992 Jan	91
3764.....	21.38000	-34.93333	RI	II-III	53	1	5	16.8	1993 May, 1991 Sep	96
3809.....	21.73000	-44.13333	IR	III	73	1	4	16.0	1993 May	84
3844.....	22.17667	-35.00000	I	II-III	52	1	5	17.0	1993 Oct	95
3864.....	22.28333	-52.73333	R	II	60	1	5	16.7	1993 Sep	88
3915.....	22.74333	-52.31667	IR	II-III	55	1	5	17.0	1993 Sep	82
3921.....	22.77500	-64.65000	R	II	93	2	5	16.9	1993 Sep	82
4010.....	23.47500	-36.78333	R	I-II	67	1	5	16.9	1991 Sep	28
4067.....	23.94000	-60.95000	R	III	72	1	5	17.1	1991 Sep	49

NOTE.—Units of right ascension are hours, and units of declination are degrees.

<sup>a</sup> Cluster classification in Abell's system: I = irregular, R = regular, IR and RI = intermediate.

<sup>b</sup> Number of cluster members between  $m_3$  and  $m_3 + 2$ , corrected for background (Abell 1958; Abell et al. 1989).

<sup>c</sup> Red magnitude of the tenth-brightest cluster member (Abell 1958; Abell et al. 1989).

<sup>d</sup> Number of galaxy velocities measured in field of cluster.

of  $\sim 2.6 \text{ \AA pixel}^{-1}$  and a final resolution of  $\sim 10 \text{ \AA}$ . The fiber images were  $\sim 8$  pixels wide and separated by  $\sim 12$  pixels from center to center.

By the time of the 1992 January observations, the Boller & Chivens spectrograph had been replaced by the “floor fiber spectrograph” built by S. Shectman. This had 128 fibers versus the original 65 but with the same wavelength coverage and resolution. At least 12 fibers out of 128 were normally dedicated to sky. The rest of the setup was the same as for the 65 fiber instrument.

As mentioned above, the front detector of the 2D-Fruitti instrument was a blue-sensitive Carnegie image tube whose output was imaged on a stack of microchannel plates. The complexities in these intermediate microchannel plate stages introduced significant position-dependent pixel-to-pixel variations, but these were independent of the object wavelength. Since no calibration in flux was intended, any wavelength-dependent

pixel-to-pixel variations of the front unit were not significant when compared to the noise introduced by the pixel-to-pixel variations of the intermediate section. Hence, quartz lamp exposures were used to correct for pixel-to-pixel variations of the detector (also known as a “flat field”). To properly illuminate the entire detector surface, and consequently the following microchannel stages, the grating angle was changed to several values during these exposures.

Helium-neon comparison lamp exposures were taken off the wind screen for wavelength calibration before and after each exposure. The 2D-Fruitti detector has a small dark current, and hence no corrections were made for that effect.

Exposure times were adjusted to be between 60 and 148 minutes, depending on the brightness of the selected galaxies for each exposure. The 2D-Fruitti instrument is a photon-counting system with which one can view the current exposure at any

TABLE 2  
VELOCITY DATA

R.A. (B1950.0) (1)	Decl. (B1950.0) (2)	Velocity (km s <sup>-1</sup> ) (3)	Error (km s <sup>-1</sup> ) (4)	$R^a$ (5)	$N^b$ (6)	$m_{\text{APM}}$ ( $b_j$ ) (7)
Abell 0080						
8.54304	-24.89661	19134	89		4	17.9
8.59467	-25.72231	18456	91	4.02		17.3
8.62092	-24.90189	19466	63	5.26		18.1
8.62167	-24.88022	19090	19	17.38		16.4
8.67258	-24.43053	26299	68		4	18.1
8.69967	-24.77514	26740	40	6.67		17.3
8.72821	-25.44467	18757	32	8.40		17.0
8.76542	-25.68603	18848	32	8.14		16.7
8.76738	-25.64111	11335	81	2.17		18.2
8.77308	-25.48561	19327	24	14.41		18.2
8.78842	-25.23067	18785	20	15.55		17.7
8.80158	-25.06683	46824	55	4.17		18.1
8.82975	-25.27392	19610	44	7.05		16.8
8.84508	-25.41200	18840	22	14.45		16.5
8.85296	-25.16981	19953	28	10.78		17.5
8.86013	-24.41097	15754	35	8.16		17.0
8.86413	-24.82242	20200	79	2.70		18.1
8.87579	-24.45431	33853	59	6.89		18.2
8.88133	-25.35728	18862	17	20.69		16.8
8.88138	-25.10375	19086	17	18.28		17.3
8.88567	-24.85181	19223	87	4.13		17.9
8.90158	-25.55344	18812	43	7.46		18.1
8.90346	-25.52053	18720	32	9.09		16.6
8.91017	-25.34245	19952	15	23.86		15.8
8.91100	-25.46392	19132	25	12.23		16.9
8.91158	-25.36586	23155	90	2.74		17.9
8.92204	-25.61689	19015	24	13.30		16.8
8.92288	-25.50572	18698	18	18.29		17.3
8.92817	-25.71933	19567	72	2.75		18.1
8.95354	-25.16981	33568	29	10.65		18.0
8.97571	-24.70645	26275	24	13.50		16.9
8.99808	-25.27289	19571	28	10.98		17.8
9.01488	-25.27667	18896	43	6.40		18.0
9.02279	-25.19039	19145	24	12.62		16.7
9.03167	-25.62456	19313	81	2.99		17.4
9.03367	-25.48383	19255	84	3.19		18.1
9.03679	-25.46317	33824	28	12.10		17.9
9.04567	-25.60708	18991	21	15.15		17.8
9.07358	-24.84483	25640	32	8.38		18.1
9.07750	-25.11583	19128	41	6.80		17.9
9.09667	-25.33556	19214	30	9.96		16.7
9.13733	-24.64961	21245	25	12.44		17.0
9.14379	-25.55219	19023	34	8.27		17.7

NOTE.—Table 2 is published in its entirety in the electronic edition of the *Astronomical Journal*. A portion is shown here for guidance regarding its form and content. Units of right ascension are hours, and units of declination are degrees.

<sup>a</sup> Redshift reliability number; see text for details.

<sup>b</sup> Number of emission or absorption lines measured; see text for details.

time. In this way one can obtain the optimum exposure time for each field. Between 28 and 196 spectra in each cluster field were obtained. See Table 1 for more details.

## 5. REDSHIFT REDUCTIONS

Radial velocity determinations were carried out using a cross-correlation technique and when necessary by identifying and fitting by eye absorption- or emission-line profiles. All reductions were performed inside the IRAF (Tody 1993) environment. For a more complete discussion of the reductions, see Quintana et al. (1996). Below is a summary of the reductions.

Due to the nature of the fiber + 2D-Frutti system, typical S-shaped distortions are inherent in this instrument. A sixth-order spline3 (Press et al. 1993, p. 106) curve was used to trace the S-shaped spectra. The IRAF HYDRA package was used to extract the spectra, correct pixel-to-pixel variations via the dome flat, use a fiber transmission table for appropriate sky subtraction, and put the spectra on a linear scale in wavelength. The wavelength solutions for 20–30 points using a fifth-, sixth-, or seventh-order Chebyshev polynomial (Press et al. 1993, p. 190) typically yielded residual rms values less than 0.4 Å, where 1 pixel  $\sim$  2.6 Å. The 10 or more sky spectra from each exposure were combined via a median filter and subtracted from each of the object spectra.

Two different methods were used to measure the redshift of the objects. For most normal early-type galaxy spectra the RVSAO (Kurtz et al. 1992) cross-correlation algorithm supported inside IRAF was used. The algorithm used in RVSAO is described in Tonry & Davis (1979, hereafter TD79). A redshift reliability/quality factor, the  $R$ -value, is generated by RVSAO (see TD79 for details). Normally, a low  $R$ -value ( $R \leq 4$ ) indicated a need to look at the spectra and try line-by-line Gaussian fitting (the second method). If the line-by-line fitting agreed to within 1  $\sigma$  of the original RVSAO result with the lowest template match error, then the RVSAO result was chosen (see next paragraph for further explanation). If it did not, then the radial velocities from each line fit were averaged, and the standard deviation became the quoted error. If there were observable emission and absorption lines, the fits were taken from the absorption lines only. All radial velocities had a heliocentric correction applied.

To use RVSAO, four template spectra set to  $z = 0$  with high S/Ns and well-determined radial velocities were used. Two of the four templates used in this paper were galaxy spectra with high S/N, NGC 1407 and NGC 1426, taken with the fiber instrument. A third template galaxy, NGC 1700, was from the previous detector on the 2.5 m at LCO (formerly known as the Sheckograph). The fourth template was a synthetic spectrum. The synthetic template was constructed from the excellent library of stellar spectra of Jacoby et al. (1984). Ratios of stellar light were used for the E0 galaxy NGC 1374 from the synthesis studies of Pickles (1985). In the end it was found that of the four radial velocity cross-correlation templates mentioned above, the template that gave the lowest error value and had  $R > 4$  provided more consistent results. It was also found that typically only one of the four templates provided values of  $R > 4$ . The cause of this behavior was related to a couple of different factors: (1) our galaxy templates were chosen to have slightly different galaxy types (E0 to E4) in order to cover the possible range of observed objects, not including AGN-type objects; and (2) the galaxy templates were observed with different instruments or synthesized. These factors resulted in different equivalent widths between galaxy templates for many of the largest absorption-line features. Hence, when a template match with  $R > 4$  was found, the others template matches had typical values of  $R \leq 4$  and inconsistent values of radial velocity.

Table 2 contains the final velocities for all members in the fields of the Abell clusters discussed in this paper. Columns (1) and (2) contain the right ascension and declination, column (3) contains the velocity, and column (4) contains the velocity error. If the value of column (4) is  $-99$ , this means that only one or two strong emission lines were found, and no estimate of the error can be given. Column (5) contains the TD79 reliability number. When column (5) is empty, column (6) contains the number of individual emission or absorption lines used in the

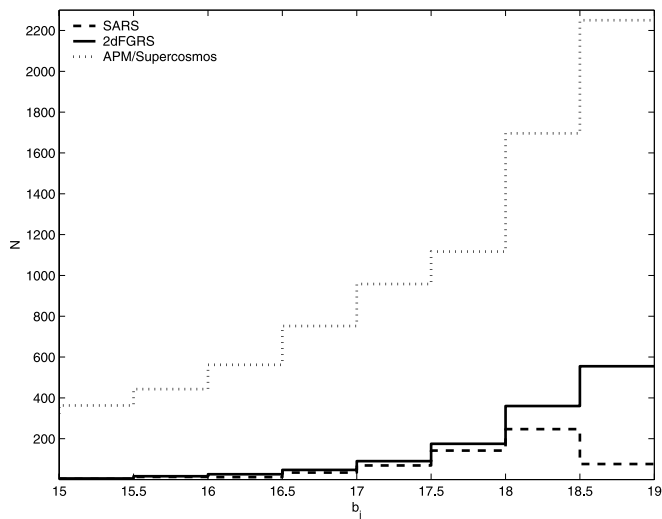


FIG. 2.—Magnitude distribution for the seven overlapping fields in the APM, 2dFGRS, and SARS samples.

velocity estimation. Column (7) contains the APM  $b_j$  magnitude of the galaxy.

#### 6. SELECTION FUNCTION, REDSHIFT COMPLETENESS, AND REDSHIFT COMPARISON

The 2dF Galaxy Redshift Survey (2dFGRS) has a carefully determined selection function (Norberg et al. 2002) based on extinction-corrected  $b_j < 19.45$  APM magnitudes. This is nearly the same as SARS, which is limited to  $15 \leq b_j < 19$ . Since seven of the SARS cluster fields (A118, A380, A2734, A2778, A2915, A2923, and A3844) overlap the 2dFGRS, the SARS redshift completeness can be evaluated against the 2dFGRS. The 2dFGRS  $b_j$  magnitudes and redshifts in the fields of these SARS clusters were obtained from the Web site interface to the 2dFGRS mSQL database.<sup>7</sup> See Colless et al. (2001, their § 9.2) for details. The relevant 2dFGRS query for this study is:

```
SELECT ra, dec, BJSEL, z, quality FROM public WHERE
extnum=0 AND quality>=3 AND BJSEL < 19.0.
```

Hence, the 2dFGRS query included only those galaxies with redshifts of quality better than 3 and  $b_j < 19$ . They also exactly overlapped a square right ascension and declination boundary in the fields of the SARS clusters.

All APM  $b_j$  magnitudes in the same overlapping regions are needed to properly characterize the SARS selection function. Hence, all the APM  $b_j$  magnitudes in the fields of the seven SARS clusters were taken from the SuperCOSMOS/APM Web site interface to the database<sup>8</sup> using the following query values: image quality, 65535; paring radius, 3"; color correct magnitudes, yes; and  $b_j < 19$ .

Figure 2 shows the  $b_j$  magnitude distribution for the APM (8140 objects for  $15 \leq b_j < 19$ ), 2dFGRS (1274 objects for  $15 \leq b_j < 19$ ), and SARS fields (596 objects) in the seven overlapping clusters.

Figure 3 demonstrates the redshift completeness as a function of  $b_j$  magnitude for the seven fields in the 2dFGRS and SARS catalogs with respect to the APM catalog (*left-hand axis*) and for SARS with respect to 2dFGRS (*right-hand axis*).

Figure 4 shows the redshift distribution of the entire SARS survey (*gray histogram*), the 2dFGRS redshifts in the seven SARS fields (*black histogram*), redshifts in the seven SARS fields that overlap the 2dFGRS (*white histogram*), and an analytical approximation curve (*gray curve*) fitted to the entire SARS survey (see text).

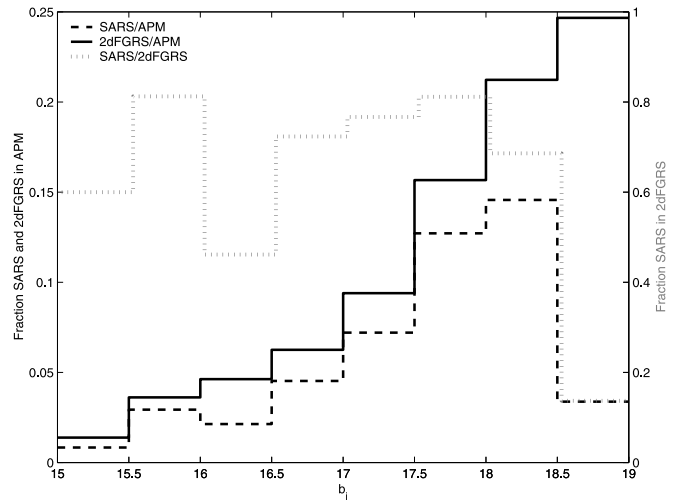


FIG. 3.—Redshift completeness for the seven overlapping fields in the APM, 2dFGRS, and SARS catalogs.

SARS fields (*black histogram*), and redshifts in the seven SARS fields that overlap the 2dFGRS (*white histogram*). A simple smooth analytic approximation curve taken from the 2dFGRS (Colless et al. 2001) is fitted to the entire SARS survey data and superposed (*gray line*). Here  $\bar{z}$  is defined as the median redshift,  $dN \propto z^2 \exp[-(1.36z/\bar{z})^{1.55}] dz$ .

It is clear from Figures 2–4 that the 2dFGRS is more complete, particularly at fainter magnitudes and redshifts, in the fields of the seven SARS clusters. Also note that the median redshift of the entire SARS catalog is  $\bar{z} = 0.0845$ , while the full 2dFGRS has a higher value of  $\bar{z} = 0.11$ .

There are several reasons for these differences. First, the 2dFGRS observed many overlapping fields to lessen the effect of fiber collisions. See Figure 15 of Colless et al. (2001) regarding the 2dFGRS redshift completeness function. This makes the 2dFGRS selection of galaxies in these fields more complete than SARS, since SARS was only able to obtain two overlapping observations in the fields of five clusters (see Table 1

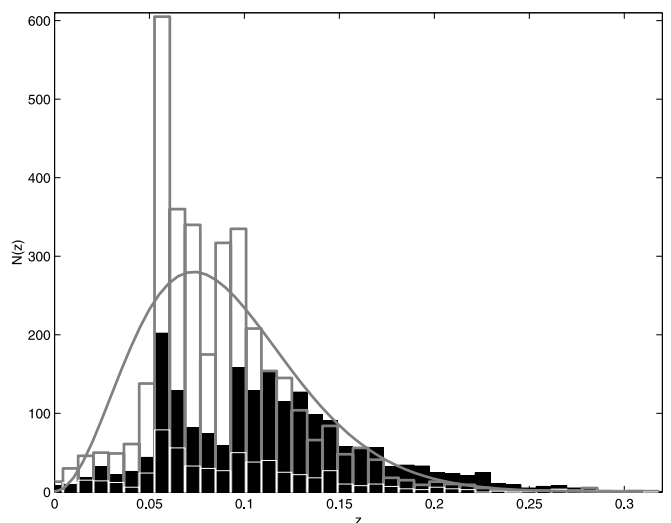


FIG. 4.—Redshift distribution of the entire SARS survey (*gray histogram*), the 2dFGRS redshifts in the seven SARS fields (*black histogram*), redshifts in the seven SARS fields that overlap the 2dFGRS (*white histogram*), and an analytical approximation curve (*gray curve*) fitted to the entire SARS survey (see text).

<sup>7</sup> See <http://www.mso.anu.edu.au/2dFGRS>.

<sup>8</sup> See <http://www.wfau.roe.ac.uk/sss/obj.html>.

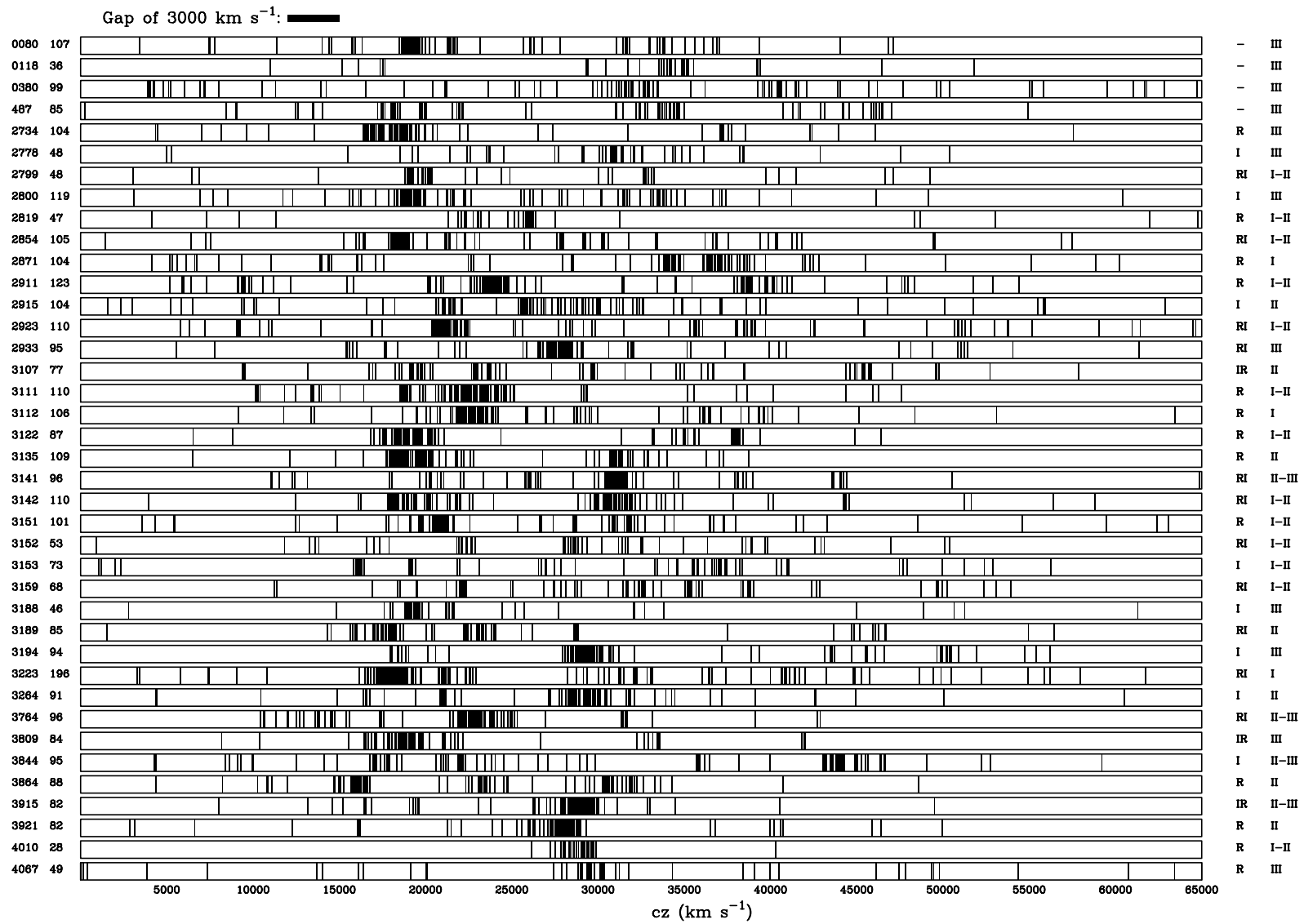


FIG. 5.—Redshift distribution for the catalog.

and Fig. 1), and none of those are in the seven 2dFGRS overlapping fields. Second, the 2dFGRS has 400 fibers spread over a  $2^\circ$  diameter field of view, whereas SARS used only either 65 fibers (2dFGRS overlap fields A118 and A2778) or 128 fibers (2dFGRS overlap fields A380, A2734, A2915, A2923, and A3844) over a  $1.5 \text{ deg}^2$  field of view. The latter is especially obvious, since the percentage difference of fibers per unit area of the 65 fiber SARS runs compared to 2dFGRS is 28.8%. For the 128 fiber SARS runs the value is 56.8%. When averaged over the total number of observed objects in the seven overlapping fields of SARS (596 objects) and 2dFGRS (1274 objects), one obtains  $596/1274 = 46.8\%$ , which is what one expects from the previous two percentages when weighted accordingly. Third is the fact that the 2dFGRS is a slightly deeper survey due to its larger aperture (4 m vs. 2.5 m) and better detector technology (CCD camera vs. a less quantum efficient photon counting system). This fact can also be seen in Figure 4 as the 2dFGRS redshifts just in the seven SARS fields (1274 objects) start to outnumber even the entire SARS survey (3440 objects) at higher redshifts. Fourth, this could also be due to the more manual selection of galaxies in the SARS survey (see § 3 above), which tried to avoid selecting foreground and background galaxies in the Abell fields. The avoidance of selecting fainter background galaxies demonstrates itself in Figures 2 and 3.

In attempting to compare the same SARS and 2dFGRS redshifts in the seven overlapping fields, one finds 530 objects that reside within  $5''$  of each other in right ascension and declination. After applying an iterative  $3\sigma$  clipping to the redshift differences of these 530 overlapping objects, 444 are left with an average redshift difference of SARS minus the 2dFGRS of  $+39.3 \text{ km s}^{-1}$ , with a standard deviation of  $138 \text{ km s}^{-1}$ .

## 7. CLUSTER IDENTIFICATION

Several authors (van Haarlem et al. 1997) have discussed the consequences of projection effects when clusters are selected in two-dimensional catalogs. Redshift surveys provide precise information on the reality of the clusters selected. Figure 5 shows the ensemble of velocities for each cluster. In several cases, the presence of a superposition of two clusters along the line of sight is obvious: A380, A2871, A2911, A3135, A3142, A3152, and A3864. Moreover, in many other cases there are more than

two concentrations along the line of sight. For example, there are three large concentrations in A2915, A3122, A3223, A3864, and A3844, including many smaller concentrations. For a more in-depth discussion of cluster identification, see Paper II.

## 8. SUMMARY

We presented a new redshift catalog of 3440 galaxies in the fields of 39 southern Abell clusters of galaxies selected from the Abell and ACO catalogs. The redshifts and corresponding APM magnitudes presented should provide a means to better characterize clusters of galaxies in the local universe when combined with the largest redshift surveys available today, the 2dFGRS (Colless et al. 2001, 2003) and the SDSS (York et al. 2000). They should also be helpful in characterizing clusters of galaxies in large-volume photometric surveys of the universe (Bahcall et al. 2003) by increasing the number of densely mapped and carefully studied clusters of galaxies.

M. J. W. acknowledges support from the NASA Ames Research Center Director's Discretionary Fund. H. Q. and L. I. acknowledge the FONDAP Centro de Astrofísica project, Chile, for partial support. H. Q. is grateful for the award of a Guggenheim Fellowship. This work was partially supported by the Consejo de Investigaciones Científicas y Técnicas de la República Argentina, CONICET, the Agencia Córdoba Ciencia, Córdoba, the Secretaría de Ciencia y Técnica, UNC, the Agencia Nacional de Promoción Científica, and the Fundación Antorchas, Argentina. The authors acknowledge the use of SuperCOSMOS Sky Survey material, which is based on photographic data originating from the UK, Palomar, and ESO Schmidt telescopes and is provided by the Wide-Field Astronomy Unit, Institute for Astronomy, University of Edinburgh. The authors also acknowledge the use of the 2dF Galaxy Redshift Survey database. The 2dF Galaxy Redshift Survey has been made possible by the dedicated efforts of the staff of the Anglo-Australian Observatory, both in creating the 2dF instrument and in supporting it on the telescope. The Anglo-Australian Observatory is funded by the Australian government (through DEST) and the UK government (through PPARC).

## REFERENCES

- Abell, G. O. 1958, *ApJS*, 3, 211  
 Abell, G. O., Corwin, H. G., Jr., & Olowin, R. P. 1989, *ApJS*, 70, 1  
 Adami, C., & Mazure, A. 2002, *A&A*, 381, 420  
 Bahcall, N., et al. 2003, *ApJS*, 148, 243  
 Bird, C. 1994, *AJ*, 107, 1637  
 Botzler, C. S., Snigula, J., Bender, R., & Hopp, U. 2004, *MNRAS*, 349, 425  
 Castillo-Morales, A., & Schindler, S. 2003, *A&A*, 403, 433  
 Coenda, V., Donzelli, C. J., Muriel, H., Quintana, H., Infante, L., & Lambas, D. G. 2005a, *AJ*, 129, 1237  
 Coenda, V., Muriel, H., Donzelli, C. J., Quintana, H., & Infante, L. 2005b, *AJ*, 129, 1237  
 Colless, M., et al. 2001, *MNRAS*, 328, 1039  
 ———. 2003, preprint (astro-ph/0306581)  
 Doroshkevich, A., Tucker, D. L., Allam, S., & Way, M. J. 2004, *A&A*, 418, 7  
 Dressler, A., & Schechtman, S. 1988, *AJ*, 95, 985  
 Fitchett, M. J. 1988, *MNRAS*, 230, 169  
 Jacoby, G. H., Hunter, D. A., & Christian, C. A. 1984, *ApJS*, 56, 257  
 Kochanek, C. S., White, M., Huchra, J., Jarrett, T. H., Schneider, S. E., & Mader, J. 2003, *ApJ*, 585, 161  
 Kurtz, M. J., Mink, D. J., Wyatt, W. F., Fabricant, D. G., Torres, G., Kriss, G. A., & Tonry, J. L. 1992, in *ASP Conf. Ser. 25, Astronomical Data Analysis Software and Systems I*, ed. D. M. Worrall, C. Biemesderfer, & J. Barnes (San Francisco: ASP), 432  
 Maddox, S. J., Sutherland, W. J., Efstathiou, G., & Loveday, J. 1990a, *MNRAS*, 243, 692  
 Maddox, S. J., Sutherland, W. J., Efstathiou, G., & Loveday, J. 1990b, *MNRAS*, 246, 433  
 ———. 1996, *MNRAS*, 283, 1227  
 Muriel, H., Quintana, H., Infante, L., Lambas, D. G., & Way, M. J. 2002, *AJ*, 124, 1934 (Paper II)  
 Norberg, P., et al. 2002, *MNRAS*, 336, 907  
 Peebles, P. J. E. 1980, *Large-Scale Structure of the Universe* (Princeton: Princeton Univ. Press)  
 Pickles, A. J. 1985, *ApJ*, 296, 340  
 Press, W. H., Teukolsky, S. A., Vetterling, W. T., & Flannery, B. P. 1993, *Numerical Recipes in C* (2nd ed.; Cambridge: Cambridge Univ. Press)  
 Quintana, H., Ramirez, A., & Way, M. J. 1996, *AJ*, 112, 36  
 Quintana, H., & White, R. A. 1990, *Ap&SS*, 173, 265  
 Schmalzing, J., Gottlöber, S., Klypin, A. A., & Kravtsov, A. V. 1999, *MNRAS*, 309, 1007  
 Shectman, S. A. 1989, *Carnegie Inst. Washington Yearb.*, 1989, 25  
 ———. 1993, in *ASP Conf. Ser. 37, Fiber Optics in Astronomy II*, ed. P. Gray (San Francisco: ASP), 26  
 Tody, D. 1993, in *ASP Conf. Ser. 52, Astronomical Data Analysis Software and Systems II*, ed. R. J. Hanisch, R. J. V. Brissenden, & J. Barnes (San Francisco: ASP), 173  
 Tonry, J., & Davis, M. 1979, *AJ*, 84, 1511 (TD79)  
 van Haarlem, M. P., Frenk, C. S., & White, S. D. M. 1997, *MNRAS*, 287, 817  
 West, M. J., & Bothun, G. D. 1990, *ApJ*, 350, 36  
 York, D. G., et al. 2000, *AJ*, 120, 1579